MDPI

Acid Resistance of Metakaolin-Based Geopolymers and Geopolymeric Mortars Reinforced with Coconut Fibers

Marco Lezzerini [1,*](ID), Andrea Aquino [2](ID) and Stefano Pagnotta [1](ID)

1   Department of Earth Sciences, University of Pisa, Via S. Maria 53, 56126 Pisa, Italy; stefano.pagnotta@unipi.it
2   Department of Geosciences, Universität Tübingen, Schnarrenbergstr. 94-96, 72076 Tübingen, Germany; andrea.aquino@uni-tuebingen.de
*   Correspondence: marco.lezzerini@unipi.it

Abstract: This paper investigates the durability of geopolymers and geopolymeric mortars made with metakaolin and alkaline activators, with and without a coconut fiber addition, after immersion for seven days into solutions of citric acid (1%, 2.5%, 5%, and 10%); hydrochloric acid (1%, 2.5%, 5%, and 10%); and sulfuric acid (1%, 2.5%, 5%, and 10%). The study focuses on mass changes, uniaxial compressive strength, flexural strength, and ultrasound pulse velocity measurements. X-ray diffraction and scanning electron microscopy are used to analyze the degradation products and microstructural changes. The aim is to assess the effect of acid exposure on the strength and stability of geopolymer materials and identify any protective effects of coconut fiber reinforcement. The samples are immersed in acid solutions of varying concentrations, and their mechanical properties are measured. The presence of coconut fibers slightly modifies the physical properties and the compressive strength, improving the mechanical flexural strength. Geopolymer and geopolymeric mortar materials experienced a weak decrease in strength when exposed to solutions of citric acid and a significant one when exposed to solutions of hydrochloric and sulfuric acids, attributed to depolymerization of the aluminosilicate binders. Brick waste geopolymeric mortars reinforced with coconut fibers showed the best performance in acid solutions with respect to geopolymers and quartz-rich sand geopolymeric mortars, suggesting a more stable cross-linked aluminosilicate geopolymer structure in this material.

Keywords: geopolymer; mortar; metakaolin; fibers; applied mineralogy; durability; acid attack

1. Introduction

In the late 1970s, Joseph Davidovits, the inventor and developer of geo-polymerization, used for the first time the term 'geopolymer' to classify a broad range of inorganic polymeric materials [1]. The geopolymer recipe depends on thermally activated natural materials like metakaolin or industrial byproducts like fly ash or slag to provide a source of silicon and aluminum. These chemical elements are dissolved in an activating alkaline solution and, subsequently, polymerize into molecular chains, becoming an interesting binding material [2]. Geopolymer is a promising binding material for its eco-friendly features and mechanical properties [3].

The widespread accessibility of raw materials and the versatility in color gradations achievable through metakaolin-based geopolymeric formulations have positioned them as viable solutions within the cultural heritage domain [4,5]. Their utilization spans a spectrum of applications, ranging from conservation and restoration endeavors to the creation of replicas and innovative artistic expressions. This convergence of material availability, color flexibility, and inherent durability underscores the significance of geopolymeric formulations in safeguarding and enhancing cultural artifacts and monuments across diverse contexts and geographies [6].

The use of geopolymers as an alternative to ordinary Portland cement (OPC) could significantly reduce the emissions of the cement industry, which amount to about 9%

CO_2 [7]; it is also interesting to note that they present better resistance to both acid attacks [8] and high temperatures [9], a more rapid strength development [10,11], low creep and shrinkage [12,13], and good durability [14–16].

Metakaolin (MK), obtained from the calcination of kaolin clay, is a common source of silica and alumina [17], and it has been used as a base material and in combination with other waste materials in the preparation of geopolymers [18–21]. Many other precursor materials can be used to create geopolymers, such as fly ash [22–25], red mud [26–28], slag [29–31], volcanic resources [32–35], waste glass [36–38], mine tailings [39–41], and different construction and demolition waste [42,43].

Since geopolymer exhibits considerable brittleness, which decreases the bending strength and favors cracks, fiber reinforcement is an effective method to improve the mechanical strength and performance of this binding material [24,44,45]. Several types of fibers have been used for different applications, such as steel, inorganic, polymeric, natural, and carbon-based fibers [46,47]. Regarding natural fibers, several works are present in the literature on the use of sisal, pineapple leaf, sweet sorghum, cotton, raffia, coir, linen, wood, bamboo, and wool fibers in the production of engineered geopolymer composites (EGCs) [48–51]. In contrast to engineered cementitious composites (ECCs), they have the dual advantage of using a low CO_2 emission geopolymeric binder and various types of fibers derived from renewable sources or recycling [52]. The addition of fibers in the formulation of geopolymer mortars creates a composite mortar with increased porosity [53], ensuring a lighter weight and improving certain physical and mechanical properties as well [54,55].

The primary purpose of this paper is the addition of coir (coconut fiber) in metakaolin geopolymers and in geopolymeric mortars to evaluate the possible improvement of their mechanical properties. Ali et al. [56], in an extensive literature review on the use of coir in cementitious materials, emphasized how this type of fiber is among those most studied for its lightness and mechanical resistance. Amalia et al. [57] proposed the use of coconut fibers to develop a geopolymer for structural engineering applications.

The present study evaluated the changes in the main physical and mechanical property values of metakaolin-based geopolymers and geopolymeric mortars due to the inclusion of coir; the effect of coconut fibers on the microstructure of these products; and their behavior when immersed into different acid solution of citric, hydrochloric, and sulfuric acids at 1%, 2.5%, 5%, and 10% concentrations.

2. Materials and Methods

2.1. The Raw Materials

In this study, high reactivity metakaolin (MK, MetaMax-BASF), the anhydrous calcined form of the kaolinite-rich clay matter, was used as an aluminosilicate material for the synthesis of geopolymer binders. The geopolymer binder (GB) was prepared by using metakaolin and an activating solution obtained by mixing sodium hydroxide (NaOH) and sodium water glass ($Na_2O \cdot SiO_2 \cdot H_2O$, 36 wt.%). Quartz-rich sand (QS) and crushed waste brick (WB) were used as aggregate materials. Coconut fibers 2 cm long, with a 1:0.01 approximative aspect ratio, were used for geopolymer and geopolymeric mortar reinforcement. To prevent the balling effect [58], the fibers were slowly introduced into the pan mixer.

2.2. Specimen Preparation

In advance, the calculated quantity as a recipe of each raw material has been prepared using a precision balance, considering that the target MK-based alkali mixture had to be composed of $Na_2O \cdot Al_2O_3 \cdot 4SiO_2 \cdot 11H_2O$. Right after, NaOH beads and Na_2SiO_3 solution have been mixed and dissolved in distilled water (Figure 1). After conducting several experiments based on the existing literature [59–61], and considering the work by Bouguermouh et al. [62], we decided to activate metakaolin with sodium silicate and hydroxide using the following molar ratios ($Al_2O_3/Na_2O = 1.0$; $SiO_2/Al_2O_3 = 3.6$ and $H_2O/Na_2O = 13.1$).

Through this iterative process, we developed a customized mix design that enables us to achieve desirable outcomes, including a well-developed pore network and appropriate setting time for both geopolymer and geopolymeric mortar, as well as excellent moldings properties. A specific amount of metakaolin was added to the NaOH and Na$_2$SiO$_3$ solution. The mixture was stirred in a laboratory planetary mixer at 2400 rpm for 10 min to achieve homogeneity, followed by stirring at 1200 rpm for 5 min to minimize the presence of bubbles. The coconut fibers were added only at the end of the mixing operations, taking care to disperse them homogeneously into the paste. The addition of both quartz sand and brick waste as aggregates was made to prepare the geopolymeric mortars. The mixtures were cast in molds (parallelepipeds: $160 \times 40 \times 40$ mm^3 and cylinders: 3 cm in diameter and 3 cm high) covered with a transparent film to avoid the rapid removal of water and cured at 60 °C for 48 h; then, they were demolded and stored at 20 °C and 85% relative humidity until the time of the tests. Testing was done after twenty-eight days in triplicate.
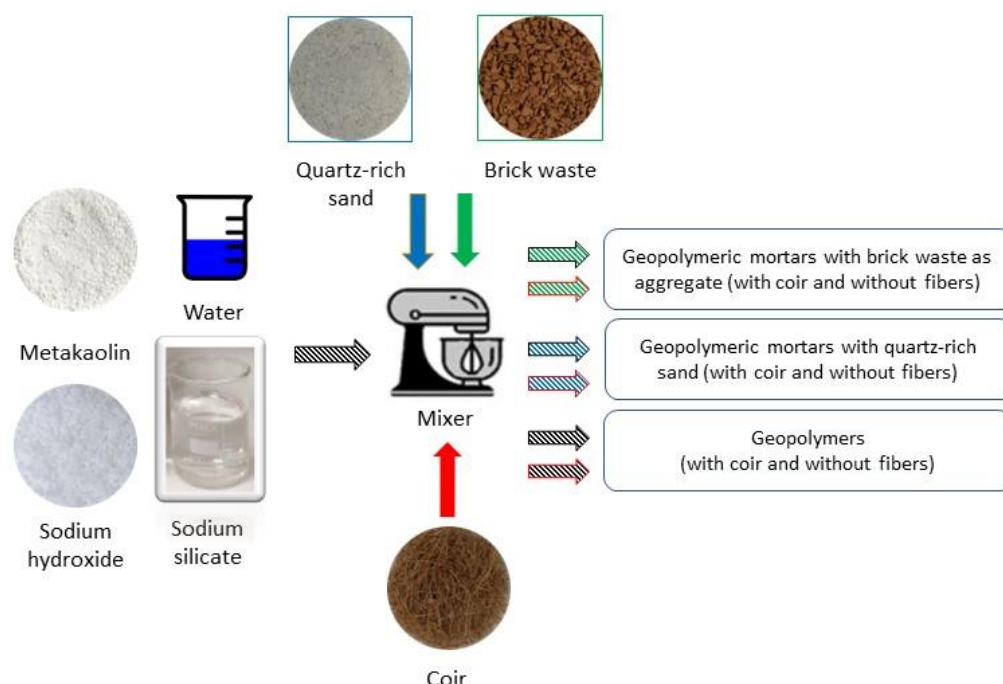
Figure 1. Procedure scheme for the preparation of both geopolymers and geopolymeric mortars starting from the raw materials used.

The geopolymer and geopolymeric mortar samples, prepared as described above, were labeled according to the temperature curing and the presence or absence of sand, brick waste, and fibers. Table 1 provides a short description of the meaning of the different labels.

Table 1. Geopolymers and geopolymeric mortar samples.

Sample	Materials
GSF	Geopolymer without fiber
GCF	Geopolymer with coconut fiber
MSF	Sand mortar without fiber
MCF	Sand mortar with coconut fiber
CSF	Brick waste mortar without fiber
CCF	Brick waste mortar with coconut fiber

2.3. Testing and Characterization

The raw materials were analyzed using XRF (ARL 9400 XP+ sequential X-ray spectrometer, Thermo Fisher Scientific S.p.A., Waltham, MA, USA) to determine their chemical

compositions, expressing the percentage content of each element in terms of oxides [63,64]. The mineralogical characterization of the raw materials was obtained by X-ray diffraction (XRD). The Bruker D2 PHASER instrument used CuKα radiation to scan the specimen's dried powder at a rate of 2°/min in the range 5–65° 2θ. Table 2 reports the chemical composition of the raw materials (metakaolin—MK, crushed waste brick—WB, and quartz-rich sand—QS).

Table 2. Chemical composition of the raw materials (mass %) by XRF.

Sample	LOI	Na$_2$O	MgO	Al$_2$O$_3$	SiO$_2$	P$_2$O$_5$	SO$_3$	K$_2$O	CaO	TiO$_2$	MnO	Fe$_2$O$_3$
MK	0.68	0.24	0.10	43.64	52.84	0.06	0.10	0.16	0.03	1.72	<0.01	0.43
WB	0.71	0.47	0.96	19.47	65.05	0.16	0.71	2.88	1.13	0.87	0.11	7.48
QS	0.33	0.10	0.22	3.16	94.57	0.03	0.01	1.34	0.06	0.05	0.01	0.12

LOI = loss on ignition at 950 °C; Fe$_2$O$_3$ = total iron expressed as Fe$_2$O$_3$.

In Figure 2, the X-ray powder diffraction (XRPD) spectra of both raw materials and products are reported. The X-ray diffraction (XRD) analysis performed on metakaolin revealed its predominant amorphous structure, with a minor presence of anatase attributable to the inherent impurities within the raw material. Conversely, the XRD patterns obtained from both the sand sample and brick waste underscored the quartz-rich composition of the former and a very low occurrence of carbonates within the latter. Considering the intended application in mortar formulations, it is imperative to note that quartz sand was used instead of river sand to improve acid resistance. Conversely, the scarce presence of carbonates within the brick waste, despite being of low concentration, may generate challenges due to their inherent susceptibility to acid-induced degradation.
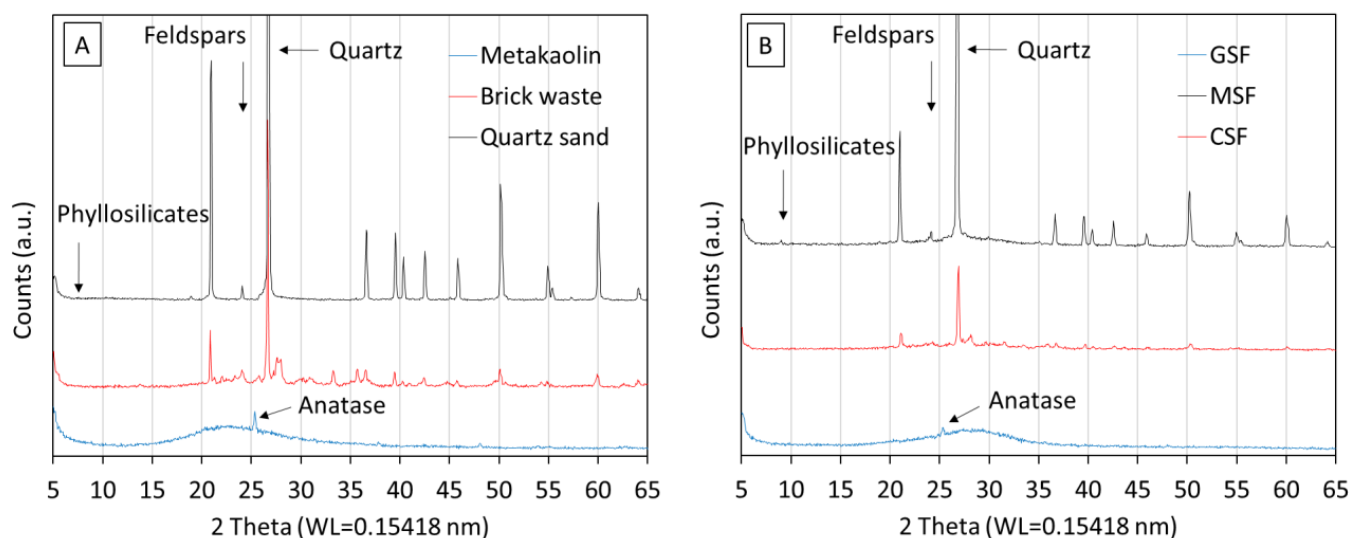
Figure 2. XRD patterns of both raw materials, (**A**) and some representative geopolymer and geopolymeric mortar samples (**B**).

To assess the microstructure of the geopolymers and geopolymeric mortar samples before and after the acid attack, field emission scanning electron microscopy (FEI Quanta 450 FEG, Center for Instrument Sharing University of Pisa–CISUP, Pisa, Italy) was used, and high-resolution images were acquired. The observations were performed under low vacuum conditions of 80 Pa and a high voltage of 5 kV, with magnification ranging from 50 to 500×.

The main physical properties (water absorption at atmospheric pressure, apparent density, and total porosity) for the geopolymer and geopolymeric mortar samples were assessed on cylindrical specimens (3 cm in diameter and 3 cm high) in accordance with

the European norms [65,66]. The volume of the specimens was measured by using the Archimedes Principle, based on the hydrostatic weighing method [67]. Before the test, the specimens were dried for 3 days at 40 °C under vacuum (Memmert GmbH + Co. KG, Schwabach, Germany vacuum oven VO 400), a temperature reported in the literature as suitable for minimizing microstructural changes in cementitious materials [68]. The total porosity of the geopolymer and geopolymeric mortar samples was determined by using the following formula: $P = (1 - G/\gamma_d) * 100$, where G and γ_d are the real density and the apparent density, respectively. The real density of the geopolymer was fixed at 2.300 g/cm^3, while that of the quartz-rich sand and waste brick was 2.650 g/cm^3.

Both the flexural strength and the uniaxial compressive strength of the hardened geopolymers and geopolymeric mortars were carried out on $160 \times 40 \times 40$ mm^3 parallelepiped specimens, in accordance with EN 1015-11:2019 [69], by using a Tecnotest 300 kN compression machine. First, the flexural test was carried out, and then, two compression tests were carried out on each prism obtained for a flexural failure of the parallelepiped itself.

Ultrasonic pulse velocity (UPV) tests were conducted by using a Proceq Pundit PL-200 instrument with 54 kHz transducers according to EN 12504-4:2021 [70] on parallelepiped specimens at 28 days of curing and on cylindrical specimens before and after the acid attack test. Three readings were taken for each specimen, and the ultrasound velocity passing through the specimen was calculated as the arithmetic mean of these readings and expressed in m/s.

The mass loss rate was calculated by referring to the following Formula (1):

$$M \,(\%) = ((m_i - m_f)/m_i) \times 100 \tag{1}$$

where M is the mass loss rate of the sample, expressed as percentage, m_i the initial mass of sample in grams, and m_f the mass of sample after acid exposure in grams.

2.4. Acid Attack Tests

Tests on cylindrical specimens (3 cm in diameter and 3 cm high) of geopolymer binders and geopolymeric mortars were done in triplicate after twenty-eight days of curing. Before the acid attacks, the samples were placed in a drying oven at 60 ± 5 °C for 24 h. This thermal treatment was applied to be sure that any absorption of water was eliminated and to facilitate the absorption of the acid solutions.

All analyzed samples were immersed at room temperature for 7 days into 1%, 2.5%, 5%, and 10% solutions of citric acid monohydrate ($C_6H_8O_7 \cdot H_2O$, >99.5%), hydrochloric acid (HCl, 37%), and sulfuric acid (H_2SO_4, 96%) inside adequately large glass containers. Every time, immediately after removal from the solution, the samples were washed in demineralized water and dried in an oven at 60 ± 5 °C for 24 h. Before and after the acid attack, the cylindrical specimens were used for evaluating changes in appearance, weight losses, and for measuring the ultrasound pulse velocities. Furthermore, optical observations, SEM, and XRD analyses were carried out.

3. Results and Discussion

3.1. Influence of Coir Addition on the Physical and Mechanical Properties of Geopolymers and Geopolymeric Mortars

The main physical properties of the geopolymers and geopolymeric mortars are reported in Table 3. The samples of geopolymer show lower apparent density and higher water absorption and porosity than those of the geopolymeric mortar ones. The presence of coconut fibers slightly modifies the physical properties and the compressive strength, improving the mechanical flexural strength (Figure 3A,B). The mechanical resistances are almost the same or slightly lower in the samples with the addition of coconut fibers. The average increase in flexural strength due to the addition of coconut fibers was 54%, 53%, and 56% for the geopolymers, geopolymeric mortar samples with quartz-rich sand, and geopolymeric mortar samples with crushed waste bricks, respectively.

Table 3. Main physical properties of the geopolymers and geopolymer mortars.

Sample	γ_d g/cm^3	Ab$_W$ wt. %	Ab$_v$ vol. %	P vol. %	SI
GSF	1.335	29.26	39.15	41.82	94
	0.005	*0.06*	*0.08*	*0.23*	*1*
GCF	1.314	29.57	38.67	43.14	90
	0.004	*0.22*	*0.20*	*0.18*	*1*
MSF	1.789	11.71	21.06	28.35	74
	0.007	*0.18*	*0.16*	*0.74*	*2*
MCF	1.790	12.27	22.12	28.17	79
	0.006	*0.07*	*0.47*	*0.54*	*3*
CSF	1.618	17.7	28.72	35.36	81
	0.004	*0.72*	*1.07*	*0.21*	*3*
CCF	1.617	18.84	30.41	35.68	85
	0.003	*0.17*	*0.34*	*0.19*	*1*

γ_d = apparent density; Ab$_W$ and Ab$_v$ = water absorption at atmospheric pressure referred to mass and to volume, respectively; P = total porosity; SI = saturation index. Average data determined on three specimens and standard deviation in italics.
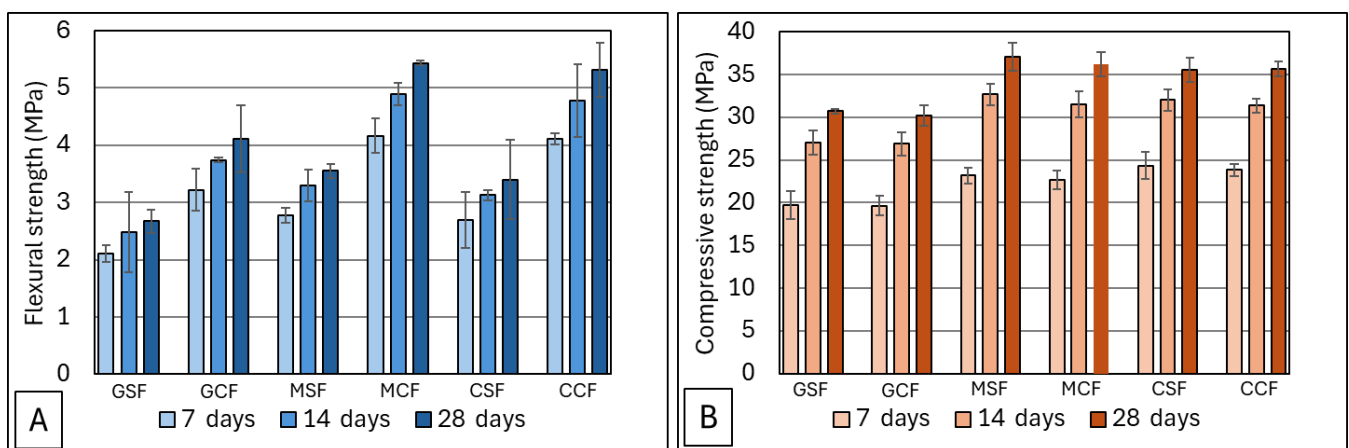

Figure 3. (**A**) Comparative values of flexural strength for geopolymers without and with coconut fibers (GSF and GCF, respectively), geopolymeric mortar samples with quartz-rich sand without and with coconut fibers (MSF and MCF, respectively), and geopolymeric mortar samples with crushed waste bricks without and with coconut fibers (CSF and CCF, respectively). (**B**) Comparative values of compressive strength for geopolymers without and with coconut fibers (GSF and GCF, respectively), geopolymeric mortar samples with quartz-rich sand without and with coconut fibers (MSF and MCF, respectively), and geopolymeric mortar samples with crushed waste bricks without and with coconut fibers (CSF and CCF, respectively).

Ayeni et al. [71] reported a similar increase in flexural strength values for a metakaolin-based geopolymer composite, although the strength values in that study were higher. In contrast, Korniejenko et al. [72] found similar flexural strength values but no increase in strength in a fly ash-based geopolymer with the addition of 1% coconut fibers. In both studies, it was observed how coconut fibers reinforce by compacting the geopolymer structure and reducing the shrinkage fractures. What likely varies is the more or less strong adhesion between the fibers and geopolymers binder.

Scanning electron microscopy (SEM) stands as a powerful technique for investigating the microstructural characteristics of geopolymer materials. This analysis enables a detailed examination of the surface morphology, particle size, distribution, and overall structural features of the geopolymers. Through high-resolution imaging and elemental analysis capabilities, SEM offers insights into the compositional variations, porosity, phase distribu-

tion, and potential defects within the geopolymers. The following section presents the SEM findings, providing a comprehensive understanding of the microstructure and composition of the studied geopolymers, crucial for elucidating their properties and applications.

In Figure 4A, the presence of shrinkage-induced fractures intersecting the closed porosity of the geopolymer is clearly visible. Additionally, a sparse closed porosity is observed, which, at the image scale ($400\times$), ranges in size from approximately 30 to 100 microns, exhibiting a perfectly spherical pore shape. As noted by Papa et al. [73], excess water that does not enter the geopolymer chain can create a steric hindrance, inducing bubble formations even with a controlled speed and mixing method. In addition to this chemical effect, the spherical pores observed in Figure 4A–C can also be attributed to a mechanical effect of air entrapment during the mixing phase. Furthermore, several clusters of salt crystals, measuring around 10 microns, are noticeable in the image, likely formed from the NaOH present in the original formulation and not involved in the geopolymerization process.
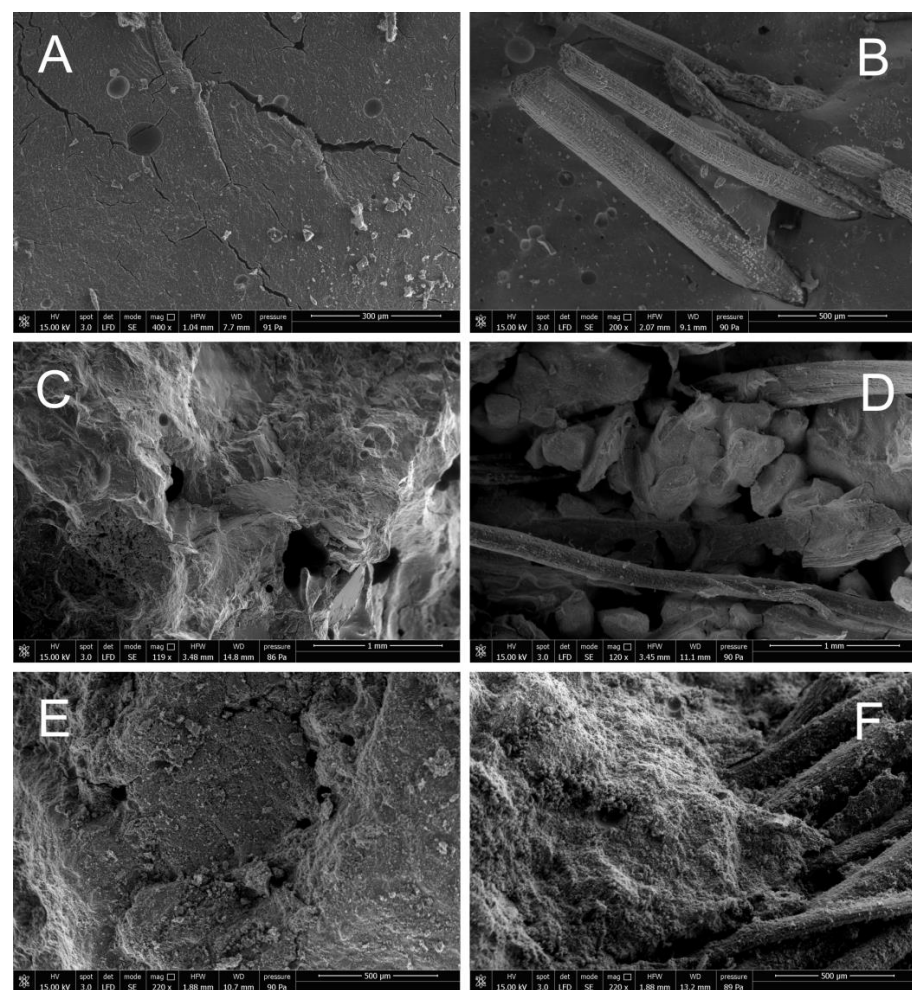
Figure 4. (**A**) SEM microphoto of the shrinkage in the geopolymer binder. (**B**) SEM microphoto of the coconut fibers in the geopolymer matrix binder. (**C**) SEM microphoto of the fracture surface of a geopolymeric mortar with quartz-rich sand. (**D**) SEM microphoto of the coconut fibers in geopolymeric mortar with quartz-rich sand. (**E**) SEM microphoto of the geopolymeric mortar with waste brick. (**F**) SEM microphoto of the coconut fibers in geopolymeric mortar with waste brick.

Regarding geopolymers reinforced with coconut fibers, as depicted in Figure 4B, the fractured surface of the binder appears smooth, displaying nearly spherical closed porosity. Small regions of salt efflorescence, of sub-nanometric dimensions, are evident, likely associated with the circulation of NaOH, which did not fully participate in the geopolymerization process. Additionally, the lumens and cell walls of the coconut fibers,

which are sub-nanometric in size, seem to have been filled by this same salt efflorescence present in the macro- and microporosity of the geopolymer, both within its structure and on its surface.

Figure 4C,D show geopolymeric mortar samples with quartz-rich sand characterized by high open porosity both in a specimen without coconut fibers and in a specimen with the addition of coconut fibers. It is possible to observe in Figure 4D a large portion of the macroporosity of the sample along the direction of the fiber visible in the lower part. Figure 4E,F show surfaces of fresh fractures covered with fine brick powder and diffuse microporosity that characterize the geopolymeric mortar samples with brick waste aggregate. Furthermore, it is noted that, in some cases, the bond between the fiber and geopolymers matrix is very strong (Figure 4F), while, in other cases, this bond appears much weaker, as highlighted by the empty space and geopolymers binder in Figure 4B; probably, the floccular structure of the geopolymers mortars has greater compatibility and adhesion to the fiber compared to the sole geopolymers binder.

3.2. Visual Inspection after Acid Attack

Visual observation of the geopolymer specimens reveals no appreciable color changes after immersion in water or acid solutions. Visual examination of the specimens immersed in water does not reveal any signs of degradation, unlike what happens when immersed in acidic substances. Figure 5 shows geopolymers and geopolymeric mortars after prolonged contact with water and immersion in acidic solutions of citric, hydrochloric, and sulfuric acid at a 10% concentration. Qu et al. [74] found chromatic alterations of the surface in the case of slag-based geopolymers and no apparent change in visual appearance for fly ash-based geopolymers, even after prolonged exposure to sulfuric acid attacks. Previously, Bakharev [8] also arrived at similar considerations by studying the behavior to an acid attack of geopolymer materials prepared with class F fly ash containing very low calcium (3–4% CaO), a material that is known to have high durability in an acidic environment.
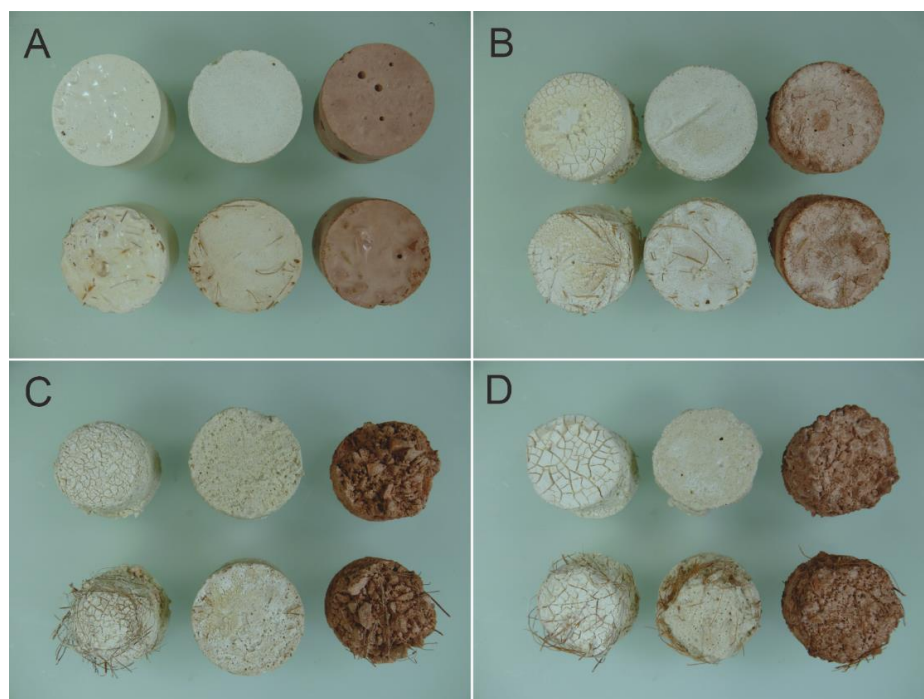
Figure 5. Comparative images of geopolymers (on the left in the pictures) and geopolymeric mortar samples with quartz-rich sand (in the middle in pictures) and brick waste aggregate (on the right in the pictures) after water absorption at atmospheric pressure (**A**) and immersion in 10% citric acid (**B**), 10% hydrochloric acid (**C**), and 10% sulfuric acid (**D**) for seven days, showing the degradation patterns.

The more acidic a solution is, the more evident the degradation of the geopolymeric materials occurs, in agreement with several previous studies [8,14,50,75]. Geopolymers appear to be easily attacked by acidic solutions, while geopolymer mortars appear to resist chemical attacks in a reasonably better way.

3.3. Loss in Mass after Acid Attack

Table 4 reports the mass changes for the specimens exposed to acid solutions (citric, hydrochloric, and sulfuric acids) for seven days. Geopolymers and geopolymeric mortars appear to be resistant to the effects of citric acid but much less to those of sulfuric and hydrochloric acids. In any case, it is evident that the mass loss increases with an increase in the acid concentration. The presence of coconut fibers slightly increases the resistance to degradation for the geopolymeric mortar samples; in contrast, it has a negative effect for the geopolymer pastes.

Table 4. Mass changes of the samples exposed to solutions of citric, hydrochloric, and sulfuric acid for 7 days at, respectively, 1%, 2.5%, 5%, and 10% concentrations.

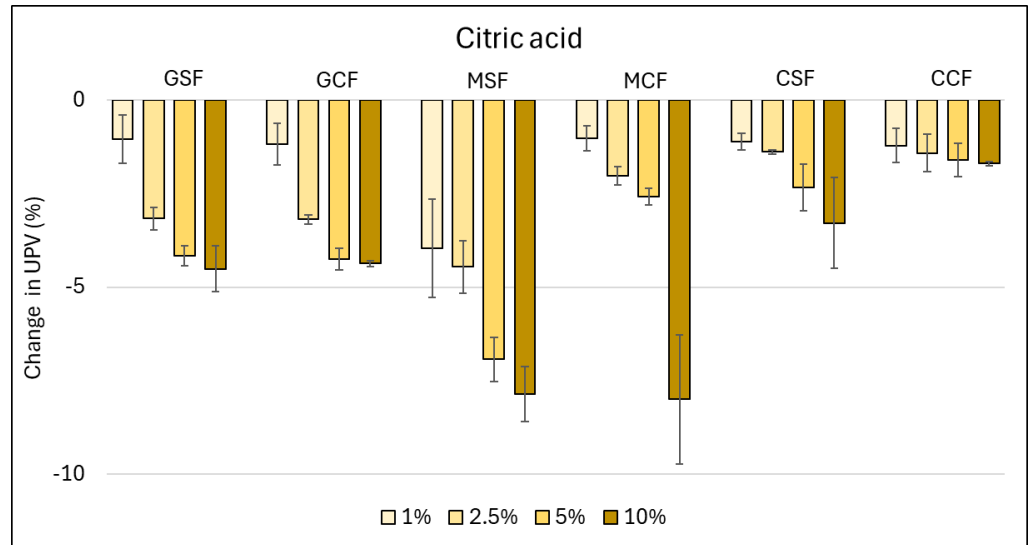| Sample	Citric Acid				Hydrochloric Acid				Sulfuric Acid			
	1% (wt. %)	2.5% (wt. %)	5% (wt. %)	10% (wt. %)	1% (wt. %)	2.5% (wt. %)	5% (wt. %)	10% (wt. %)	1% (wt. %)	2.5% (wt. %)	5% (wt. %)	10% (wt. %)
GSF	−1.16	−1.35	−1.87	−2.62	−2.74	−5.96	14.13	22.24	−4.41	−8.72	18.20	26.09
	0.16	*0.08*	*0.07*	*0.28*	*0.62*	*0.23*	*0.89*	*0.31*	*0.29*	*0.37*	*0.23*	*1.08*
GCF	−0.93	−1.23	−1.84	−2.65	−4.89	−7.61	15.40	23.02	−4.87	−9.40	19.37	30.08
	0.23	*0.17*	*0.08*	*0.45*	*0.28*	*0.22*	*0.84*	*0.36*	*0.40*	*0.62*	*0.31*	*0.85*
MSF	−0.40	−0.53	−1.08	−1.98	−0.62	−2.67	−4.74	−6.57	−4.30	−5.02	−6.19	−7.52
	0.14	*0.12*	*0.17*	*0.28*	*0.13*	*0.12*	*0.49*	*0.43*	*0.35*	*0.22*	*0.31*	*0.37*
MCF	−0.72	−0.84	−1.06	−1.51	−2.10	−3.85	−4.57	−5.00	−4.79	−5.07	−5.95	−6.21
	0.04	*0.05*	*0.17*	*0.02*	*0.29*	*0.16*	*0.25*	*0.25*	*0.12*	*0.09*	*0.19*	*0.29*
CSF	−1.25	−1.40	−1.68	−2.12	−0.56	−1.86	−3.86	−6.02	−2.76	−3.36	−4.83	−6.32
	0.13	*0.14*	*0.04*	*0.16*	*0.03*	*0.17*	*0.12*	*0.26*	*0.19*	*0.08*	*0.07*	*0.13*
CCF	−0.77	−0.93	−0.99	−1.26	−1.99	−2.87	−3.36	−3.76	−2.66	−2.99	−3.78	−4.66
	0.15	*0.12*	*0.30*	*0.11*	*0.12*	*0.10*	*0.30*	*0.17*	*0.04*	*0.30*	*0.15*	*0.30*

Average data determined on three specimens and standard deviation in italics.

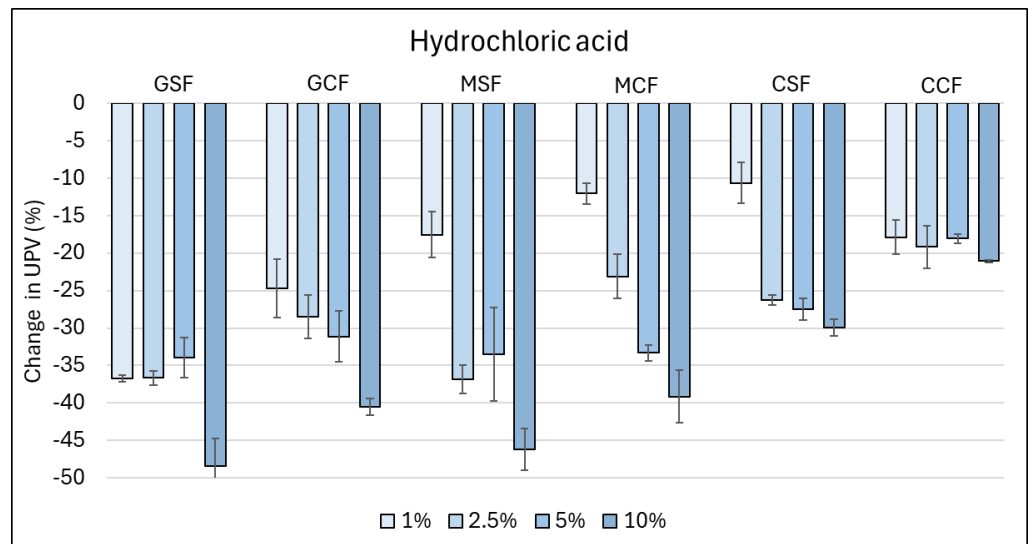### 3.4. Ultrasound Pulse Velocity after Acid Attack

Figures 6–8 present the results of the ultrasonic pulse velocity (UPV) analysis conducted on selected geopolymer and geopolymeric mortar specimens following exposure to an acid attack. This nondestructive testing method offers valuable insights into the structural integrity and physicomechanical conditions of materials by measuring the velocity of ultrasonic pulses propagating through them. The use of UPV is due to the need to analyze samples that become rather fragile due to acid attacks. This nondestructive and highly portable methodology allows for the analysis of the mechanical properties of a geomaterial through simple contact. Furthermore, the results obtained from UPV are well correlated with the mechanical properties of the material, especially with the compressive strength [76].

The graphs almost always illustrate a decreasing trend in the percentage of UPV for both the geopolymer and geopolymeric mortar specimens after exposure to an acid attack. This decrease indicates a deterioration of the physical and mechanical properties, likely attributed to chemical interactions between the acids and the constituents of the samples. Geopolymers demonstrated a heightened resistance to acid aggression, owing to the inherent acid-resistant characteristics conferred by accessory minerals present in the raw materials, notably quartz and clay minerals, as corroborated by prior findings documented by Bouguermouh et al. [62]. This principle extends to the minerals within the aggregate utilized in geopolymer mortar fabrication: mortars composed of quartz-based aggregates manifest augmented resilience to acid attacks, whereas the inclusion of carbonate minerals may exacerbate its susceptibility. A notable observation is the correlation between the acid concentration and the extent of the damage, as evidenced by the low ultrasound speed in the samples subjected to high acid concentrations. This relationship underscores the

heightened aggressiveness of acidic environments and their detrimental effects on the structural integrity of the geopolymeric materials. However, the presence of coconut fibers enhances the structural integrity in geopolymer systems, though, in certain instances, they may act as capillaries on the sample's external surface, facilitating acid penetration into the geopolymer. The test results highlight the varying degrees of resilience exhibited by geopolymer and geopolymeric mortar specimens against different acid attacks.

Figure 6. Images showing the decreasing of the ultrasound pulse velocity after a citric acid attack for the analyzed samples.

Figure 7. Images showing the decreasing of the ultrasound pulse velocity after a hydrochloric acid attack for the analyzed samples.

The statistical analysis of the data collected, despite the small number of samples analyzed in each sample category, suggests the presence of linear correlations between the physical and mechanical parameters. In fact, it is possible to observe good correlations among the apparent density, water absorption, porosity, ultrasound pulse velocity, and uniaxial compressive strength. Regarding the acid attacks, excluding the data of citric acid exposure that caused a weak deterioration, it is possible to note high correlation values ($R^2 > |0.8|$) between the mass changes and UPVs for the geopolymeric mortar samples. The observed deterioration in the UPV underscores the critical importance of

developing geopolymeric materials with enhanced acid resistance [67]. Such materials could find widespread utility in infrastructure projects, where exposure to acidic substances, such as industrial effluents or environmental pollutants, poses a significant challenge to conventional construction materials.
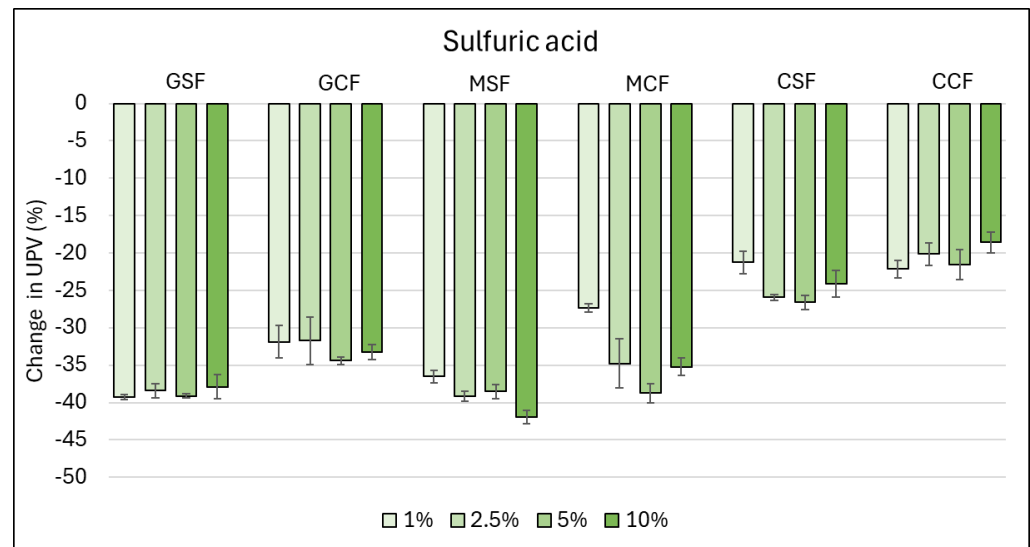
Figure 8. Images showing the decreasing of the ultrasound pulse velocity after a sulfuric acid attack for the analyzed samples.

4. Conclusions

Incorporating coconut fibers into geopolymeric materials brings notable improvements in several key properties. The addition of 2% coconut fibers significantly enhances the flexural strength by up to 56%, although its impact on the compressive strength seems minimal. Analyzing further, we found that coconut fibers increase the water ingress in both geopolymer matrices and mortars, with a slight decrease in the saturation indices in matrices but an increase in mortars. This heightened permeation exacerbates moisture absorption, attributed to the capillary action of coconut fibers. Despite this, incorporating coconut fibers into sand-based and brick powder-based geopolymeric mortars modestly boosts their hydraulicity index and flexural strength while also providing protection against acid degradation, thereby extending their durability. Future research should optimize their chemical composition and formulation to enhance acid resistance, possibly through additives or modified curing conditions. Exploring reinforcement techniques like coconut fiber reinforcement shows promise in improving their acid resistance and overall durability. Ultrasonic pulse velocity analysis offers valuable insights into material performance under acidic conditions, contributing significantly to advancing resilient geopolymeric materials in engineering and construction applications.

References

1. Davidovits, J. *Geopolymer Chemistry and Applications*; Geopolymer Institute: Saint-Quentin, France, 2008.
2. Aleem, M.I.A.; Arumairaj, P.D. Geopolymer concrete—A review. *Int. J. Eng. Sci. Emerg. Technol.* **2012**, *1*, 118–122. [CrossRef]
3. Cong, P.; Cheng, Y. Advances in geopolymer materials: A comprehensive review. *J. Traffic Transp. Eng. (Engl. Ed.)* **2021**, *8*, 283–314. [CrossRef]
4. Ricciotti, L.; Molino, A.J.; Roviello, V.; Chianese, E.; Cennamo, P.; Roviello, G. Geopolymer composites for potential applications in cultural heritage. *Environments* **2017**, *4*, 91. [CrossRef]
5. Pagnotta, S.; Tenorio, A.L.; Tinè, M.R.; Lezzerini, M. Geopolymer mortar: Metakaolin-based recipe for cultural heritage application. In Proceedings of the 2020 IMEKO TC-4 International Conference on Metrology for Archaeology and Cultural Heritage, Trento, Italy, 22–24 October 2020; pp. 55–59.
6. Pagnotta, S.; Lluveras Tenorio, A.; Tinè, M.R.; Aquino, A.; Lezzerini, M. Geopolymers as a potential material for preservation and restoration of Urban Build Heritage: An overview. *IOP Conf. Ser. Earth Environ. Sci.* **2020**, *609*, 12057. [CrossRef]
7. Si, R.; Dai, Q.; Guo, S.; Wang, J. Mechanical property, nanopore structure and drying shrinkage of metakaolin-based geopolymer with waste glass powder. *J. Clean. Prod.* **2020**, *242*, 118502. [CrossRef]
8. Bakharev, T. Resistance of geopolymer materials to acid attack. *Cem. Concr. Res.* **2005**, *35*, 658–670. [CrossRef]
9. Kong, D.L.Y.; Sanjayan, J.G. Damage behavior of geopolymer composites exposed to elevated temperatures. *Cem. Concr. Compos.* **2008**, *30*, 986–991. [CrossRef]
10. Nurruddin, M.F.; Sani, H.; Mohammed, B.S.; Shaaban, I. Methods of curing geopolymer concrete: A review. *Int. J. Adv. Appl. Sci.* **2018**, *5*, 31–36. [CrossRef]
11. Hawa, A.; Tonnayopas, D.; Prachasaree, W.; Taneerananon, P. Development and performance evaluation of very high early strength geopolymer for rapid road repair. *Adv. Mater. Sci. Eng.* **2013**, *2013*, 764180. [CrossRef]
12. Wallah, S.E. Creep behaviour of fly ash-based geopolymer concrete. *Civ. Eng. Dimens.* **2010**, *12*, 73–78.
13. Sagoe-Crentsil, K.; Brown, T.; Taylor, A. Drying shrinkage and creep performance of geopolymer concrete. *J. Sustain. Cem. Mater.* **2013**, *2*, 35–42. [CrossRef]
14. Chen, K.; Wu, D.; Xia, L.; Cai, Q.; Zhang, Z. Geopolymer concrete durability subjected to aggressive environments—A review of influence factors and comparison with ordinary Portland cement. *Constr. Build. Mater.* **2021**, *279*, 122496. [CrossRef]
15. Niveditha, M.; Koniki, S. Effect of Durability properties on Geopolymer concrete—A Review. *E3S Web Conf.* **2020**, *184*, 1092. [CrossRef]
16. Amran, M.; Al-Fakih, A.; Chu, S.H.; Fediuk, R.; Haruna, S.; Azevedo, A.; Vatin, N. Long-term durability properties of geopolymer concrete: An in-depth review. *Case Stud. Constr. Mater.* **2021**, *15*, e00661. [CrossRef]
17. Siddique, R.; Klaus, J. Influence of metakaolin on the properties of mortar and concrete: A review. *Appl. Clay Sci.* **2009**, *43*, 392–400. [CrossRef]
18. Jindal, B.B.; Alomayri, T.; Hasan, A.; Kaze, C.R. Geopolymer concrete with metakaolin for sustainability: A comprehensive review on raw material's properties, synthesis, performance, and potential application. *Environ. Sci. Pollut. Res.* **2022**, 1–26. [CrossRef] [PubMed]
19. Kim, B.; Lee, S. Review on characteristics of metakaolin-based geopolymer and fast setting. *J. Korean Ceram. Soc.* **2020**, *57*, 368–377. [CrossRef]
20. Lahoti, M.; Wong, K.K.; Yang, E.-H.; Tan, K.H. Effects of Si/Al molar ratio on strength endurance and volume stability of metakaolin geopolymers subject to elevated temperature. *Ceram. Int.* **2018**, *44*, 5726–5734. [CrossRef]
21. Pagnotta, S.; Lezzerini, M. Comparison Between LEEB And Knoop Hardness On Metakaolin-Based Geopolymer. *Atti Soc. Tosc. Sci. Nat. Mem. Ser. A* **2020**, *127*, 67–73. [CrossRef]
22. Junaid, M.T.; Kayali, O.; Khennane, A.; Black, J. A mix design procedure for low calcium alkali activated fly ash-based concretes. *Constr. Build. Mater.* **2015**, *79*, 301–310. [CrossRef]
23. Pan, Z.; Tao, Z.; Cao, Y.F.; Wuhrer, R.; Murphy, T. Compressive strength and microstructure of alkali-activated fly ash/slag binders at high temperature. *Cem. Concr. Compos.* **2018**, *86*, 9–18. [CrossRef]
24. Gailitis, R.; Sprince, A.; Kozlovskis, T.; Radina, L.; Pakrastins, L.; Vatin, N. Long-term properties of different fiber reinforcement effect on fly ash-based geopolymer composite. *Crystals* **2021**, *11*, 760. [CrossRef]
25. Fan, F.; Liu, Z.; Xu, G.; Peng, H.; Cai, C.S. Mechanical and thermal properties of fly ash based geopolymers. *Constr. Build. Mater.* **2018**, *160*, 66–81. [CrossRef]
26. Zhang, G.; He, J.; Gambrell, R.P. Synthesis, characterization, and mechanical properties of red mud–based geopolymers. *Transp. Res. Rec.* **2010**, *2167*, 1–9. [CrossRef]

27. Qaidi, S.M.A.; Tayeh, B.A.; Ahmed, H.U.; Emad, W. A review of the sustainable utilisation of red mud and fly ash for the production of geopolymer composites. *Constr. Build. Mater.* **2022**, *350*, 128892. [CrossRef]

28. Kumar, A.; Saravanan, T.J.; Bisht, K.; Kabeer, K.I.S.A. A review on the utilization of red mud for the production of geopolymer and alkali activated concrete. *Constr. Build. Mater.* **2021**, *302*, 124170. [CrossRef]

29. Cheng, T.-W.; Chiu, J.P. Fire-resistant geopolymer produced by granulated blast furnace slag. *Miner. Eng.* **2003**, *16*, 205–210. [CrossRef]

30. Qaidi, S.M.A.; Tayeh, B.A.; Isleem, H.F.; de Azevedo, A.R.G.; Ahmed, H.U.; Emad, W. Sustainable utilization of red mud waste (bauxite residue) and slag for the production of geopolymer composites: A review. *Case Stud. Constr. Mater.* **2022**, *16*, e00994. [CrossRef]

31. Zhang, P.; Gao, Z.; Wang, J.; Guo, J.; Hu, S.; Ling, Y. Properties of fresh and hardened fly ash/slag based geopolymer concrete: A review. *J. Clean. Prod.* **2020**, *270*, 122389. [CrossRef]

32. Djobo, J.N.Y.; Elimbi, A.; Tchakouté, H.K.; Kumar, S. Mechanical properties and durability of volcanic ash based geopolymer mortars. *Constr. Build. Mater.* **2016**, *124*, 606–614. [CrossRef]

33. Pulidori, E.; Lluveras-Tenorio, A.; Carosi, R.; Bernazzani, L.; Duce, C.; Pagnotta, S.; Lezzerini, M.; Barone, G.; Mazzoleni, P.; Tiné, M.R. Building geopolymers for CuHe part I: Thermal properties of raw materials as precursors for geopolymers. *J. Therm. Anal. Calorim.* **2022**, *147*, 5323–5335. [CrossRef]

34. Pelosi, C.; Occhipinti, R.; Finocchiaro, C.; Lanzafame, G.; Pulidori, E.; Lezzerini, M.; Barone, G.; Mazzoleni, P.; Tiné, M.R. Thermal and morphological investigations of alkali activated materials based on Sicilian volcanic precursors (Italy). *Mater. Lett.* **2023**, *335*, 133773. [CrossRef]

35. Zeyad, A.M.; Magbool, H.M.; Tayeh, B.A.; de Azevedo, A.R.G.; Abutaleb, A.; Hussain, Q. Production of geopolymer concrete by utilizing volcanic pumice dust. *Case Stud. Constr. Mater.* **2022**, *16*, e00802. [CrossRef]

36. Çelik, A.İ.; Tunç, U.; Bahrami, A.; Karalar, M.; Mydin, M.A.O.; Alomayri, T.; Özkılıç, Y.O. Use of waste glass powder toward more sustainable geopolymer concrete. *J. Mater. Res. Technol.* **2023**, *24*, 8533–8546. [CrossRef]

37. Xiao, R.; Huang, B.; Zhou, H.; Ma, Y.; Jiang, X. A state-of-the-art review of crushed urban waste glass used in OPC and AAMs (geopolymer): Progress and challenges. *Clean. Mater.* **2022**, *4*, 100083. [CrossRef]

38. Tahwia, A.M.; Heniegal, A.M.; Abdellatief, M.; Tayeh, B.A.; Abd Elrahman, M. Properties of ultra-high performance geopolymer concrete incorporating recycled waste glass. *Case Stud. Constr. Mater.* **2022**, *17*, e01393. [CrossRef]

39. He, X.; Yuhua, Z.; Qaidi, S.; Isleem, H.F.; Zaid, O.; Althoey, F.; Ahmad, J. Mine tailings-based geopolymers: A comprehensive review. *Ceram. Int.* **2022**, *48*, 24192–24212. [CrossRef]

40. Zhang, N.; Hedayat, A.; Figueroa, L.; Steirer, K.X.; Li, L.; Sosa, H.G.B. Physical, mechanical, cracking, and damage properties of mine tailings-based geopolymer: Experimental and numerical investigations. *J. Build. Eng.* **2023**, *75*, 107075. [CrossRef]

41. Qaidi, S.M.A.; Tayeh, B.A.; Zeyad, A.M.; de Azevedo, A.R.G.; Ahmed, H.U.; Emad, W. Recycling of mine tailings for the geopolymers production: A systematic review. *Case Stud. Constr. Mater.* **2022**, *16*, e00933. [CrossRef]

42. Gu, F.; Xie, J.; Vuye, C.; Wu, Y.; Zhang, J. Synthesis of geopolymer using alkaline activation of building-related construction and demolition wastes. *J. Clean. Prod.* **2023**, *420*, 138335. [CrossRef]

43. Ozcelikci, E.; Kul, A.; Gunal, M.F.; Ozel, B.F.; Yildirim, G.; Ashour, A.; Sahmaran, M. A comprehensive study on the compressive strength, durability-related parameters and microstructure of geopolymer mortars based on mixed construction and demolition waste. *J. Clean. Prod.* **2023**, *396*, 136522. [CrossRef]

44. Ranjbar, N.; Zhang, M. Fiber-reinforced geopolymer composites: A review. *Cem. Concr. Compos.* **2020**, *107*, 103498. [CrossRef]

45. Camargo, M.M.; Adefrs Taye, E.; Roether, J.A.; Tilahun Redda, D.; Boccaccini, A.R. A review on natural fiber-reinforced geopolymer and cement-based composites. *Materials* **2020**, *13*, 4603. [CrossRef] [PubMed]

46. Samal, S.; Blanco, I. An Application Review of Fiber-Reinforced Geopolymer Composite. *Fibers* **2021**, *9*, 23. [CrossRef]

47. Korniejenko, K.; Łach, M.; Mikuła, J. The influence of short coir, glass and carbon fibers on the properties of composites with geopolymer matrix. *Materials* **2021**, *14*, 4599. [CrossRef] [PubMed]

48. Silva, G.; Kim, S.; Aguilar, R.; Nakamatsu, J. Natural fibers as reinforcement additives for geopolymers—A review of potential eco-friendly applications to the construction industry. *Sustain. Mater. Technol.* **2020**, *23*, e00132. [CrossRef]

49. Furtos, G.; Molnar, L.; Silaghi-Dumitrescu, L.; Pascuta, P.; Korniejenko, K. Mechanical and thermal properties of wood fiber reinforced geopolymer composites. *J. Nat. Fibers* **2022**, *19*, 6676–6691. [CrossRef]

50. Sá Ribeiro, M.G.; Sá Ribeiro, M.G.; Keane, P.F.; Sardela, M.R.; Kriven, W.M.; Sá Ribeiro, R.A. Acid resistance of metakaolin-based, bamboo fiber geopolymer composites. *Constr. Build. Mater.* **2021**, *302*, 124194. [CrossRef]

51. Natali Murri, A.; Medri, V.; Landi, E. Production and thermomechanical characterization of wool–geopolymer composites. *J. Am. Ceram. Soc.* **2017**, *100*, 2822–2831. [CrossRef]

52. Zhong, H.; Zhang, M. Engineered geopolymer composites: A state-of-the-art review. *Cem. Concr. Compos.* **2023**, *135*, 104850. [CrossRef]

53. Zhang, X.; Bai, C.; Qiao, Y.; Wang, X.; Jia, D.; Li, H.; Colombo, P. Porous geopolymer composites: A review. *Compos. Part A Appl. Sci. Manuf.* **2021**, *150*, 106629. [CrossRef]

54. Shaikh, F.U.A. Review of mechanical properties of short fibre reinforced geopolymer composites. *Constr. Build. Mater.* **2013**, *43*, 37–49. [CrossRef]

55. Farhan, K.Z.; Johari, M.A.M.; Demirboğa, R. Impact of fiber reinforcements on properties of geopolymer composites: A review. *J. Build. Eng.* **2021**, *44*, 102628. [CrossRef]
56. Ali, B.; Hawreen, A.; Ben Kahla, N.; Talha Amir, M.; Azab, M.; Raza, A. A critical review on the utilization of coir (coconut fiber) in cementitious materials. *Constr. Build. Mater.* **2022**, *351*, 128957. [CrossRef]
57. Amalia, F.; Akifah, N. Development of coconut trunk fiber geopolymer hybrid composite for structural engineering materials. *IOP Conf. Ser. Mater. Sci. Eng.* **2017**, *180*, 12014. [CrossRef]
58. Zakaria, M.; Ahmed, M.; Hoque, M.M.; Islam, S. Scope of using jute fiber for the reinforcement of concrete material. *Text. Cloth. Sustain.* **2017**, *2*, 123. [CrossRef]
59. Driouich, A.; Chajri, F.; El Hassani, S.E.A.; Britel, O.; Belouafa, S.; Khabbazi, A.; Chaair, H. Optimization synthesis geopolymer based mixture metakaolin and fly ash activated by alkaline solution. *J. Non. Cryst. Solids* **2020**, *544*, 120197. [CrossRef]
60. Liu, J.; Doh, J.-H.; Dinh, H.L.; Ong, D.E.L.; Zi, G.; You, I. Effect of Si/Al molar ratio on the strength behavior of geopolymer derived from various industrial waste: A current state of the art review. *Constr. Build. Mater.* **2022**, *329*, 127134. [CrossRef]
61. Li, N.; Shi, C.; Zhang, Z.; Wang, H.; Liu, Y. A review on mixture design methods for geopolymer concrete. *Compos. Part B Eng.* **2019**, *178*, 107490. [CrossRef]
62. Bouguermouh, K.; Bouzidi, N.; Mahtout, L.; Pérez-Villarejo, L.; Martínez-Cartas, M.L. Effect of acid attack on microstructure and composition of metakaolin-based geopolymers: The role of alkaline activator. *J. Non. Cryst. Solids* **2017**, *463*, 128–137. [CrossRef]
63. Lezzerini, M.; Tamponi, M.; Bertoli, M. Reproducibility, precision and trueness of X-ray fluorescence data for mineralogical and/or petrographic purposes. *Atti Soc. Tosc. Sci. Nat. Mem. Ser. A* **2013**, *120*, 67–73. [CrossRef]
64. Lezzerini, M.; Tamponi, M.; Bertoli, M. Calibration of XRF data on silicate rocks using chemicals as in-house standards. *Atti Soc. Tosc. Sci. Nat. Mem. Ser. A* **2014**, *121*, 65–70.
65. *EN 1925*; Natural Stone Test Methods—Determination of Water Absorption Coefficient by Capillary. European Committee for Standardization (CEN): Brussels, Belgium, 1999.
66. *EN 1936*; Natural Stone Test Methods—Determination of Real Density and Apparent Density, and of Total and Open Porosity. European Committee for Standardization (CEN): Brussels, Belgium, 2006.
67. Franzini, M.; Lezzerini, M. A mercury-displacement method for stone bulk-density determinations. *Eur. J. Mineral.* **2003**, *15*, 225–229. [CrossRef]
68. Trincal, V.; Benavent, V.; Lahalle, H.; Balsamo, B.; Samson, G.; Patapy, C.; Jainin, Y.; Cyr, M. Effect of drying temperature on the properties of alkali-activated binders-Recommendations for sample preconditioning. *Cem. Concr. Res.* **2022**, *151*, 106617. [CrossRef]
69. *EN 1015-11*; Methods of Test for Mortar for Masonry—Part 11: Determination of Flexural and Compressive Strength of Hardened Mortar. European Committee for Standardization (CEN): Brussels, Belgium, 2019; pp. 1–15.
70. *EN 12504-4*; Testing Concrete—Part 4: Determination of Ultrasonic Pulse Velocity. European Committee for Standardization (CEN): Brussels, Belgium, 2004.
71. Ayeni, O.; Mahamat, A.A.; Bih, N.L.; Stanislas, T.T.; Isah, I.; Savastano Junior, H.; Boakye, E.; Onwualu, A.P. Effect of Coir Fiber Reinforcement on Properties of Metakaolin-Based Geopolymer Composite. *Appl. Sci.* **2022**, *12*, 5478. [CrossRef]
72. Korniejenko, K.; Frączek, E.; Pytlak, E.; Adamski, M. Mechanical properties of geopolymer composites reinforced with natural fibers. *Procedia Eng.* **2016**, *151*, 388–393. [CrossRef]
73. Papa, E.; Medri, V.; Landi, E.; Ballarin, B.; Miccio, F. Production and characterization of geopolymers based on mixed compositions of metakaolin and coal ashes. *Mater. Des.* **2014**, *56*, 409–415. [CrossRef]
74. Qu, F.; Li, W.; Wang, K.; Zhang, S.; Sheng, D. Performance deterioration of fly ash/slag-based geopolymer composites subjected to coupled cyclic preloading and sulfuric acid attack. *J. Clean. Prod.* **2021**, *321*, 128942. [CrossRef]
75. Duan, P.; Yan, C.; Zhou, W.; Luo, W.; Shen, C. An investigation of the microstructure and durability of a fluidized bed fly ash-metakaolin geopolymer after heat and acid exposure. *Mater. Des.* **2015**, *74*, 125–137. [CrossRef]
76. Vasanelli, E.; Colangiuli, D.; Calia, A.; Sileo, M.; Aiello, M.A. Ultrasonic pulse velocity for the evaluation of physical and mechanical properties of a highly porous building limestone. *Ultrasonics* **2015**, *60*, 33–40. [CrossRef]